

Ghost imaging with a single detector

Yaron Bromberg[†], Ori Katz[†], and Yaron Silberberg^{*}

Department of Physics of Complex Systems, the Weizmann Institute of Science, Rehovot, Israel

We experimentally demonstrate pseudothermal ghost-imaging and ghost-diffraction using only a single single-pixel detector. We achieve this by replacing the high resolution detector of the reference beam with a computation of the propagating field, following a recent proposal by Shapiro [J. H. Shapiro, arXiv:0807.2614 (2008)]. Since only a single detector is used, this provides an experimental evidence that pseudothermal ghost imaging does not rely on non-local quantum correlations. In addition, we show the depth-resolving capability of this ghost-imaging technique.

In ghost imaging (GI) an object is imaged even though the light which illuminates it is collected by a single-pixel detector which has no spatial resolution (a bucket detector). This is done by using two spatially correlated beams. One of the beams illuminates the object, and the photons transmitted by the object are collected by the bucket detector. The other beam impinges on a multipixel detector (e.g. a CCD camera), without ever passing through the object (the reference beam). Nevertheless, by correlating the intensities measured by the bucket detector with the intensities of each pixel in the multipixel detector, an image of the object is reconstructed [1]. In a similar fashion, the diffraction pattern of the object can also be obtained ('ghost diffraction', GD). In the first demonstrations of GI and GD the two beams were formed from a stream of entangled photons [2, 3]. The reconstruction of the image was attributed to the non-local quantum correlations between the photon pairs. Challenging this interpretation, Bennik *et al.* demonstrated GI using two classically correlated beams [4], and triggered an ongoing effort to clarify the role of entanglement in GI and GD [5, 6, 7, 8, 9, 10, 11, 12, 13, 14]. It was soon discovered that many of the features obtained with entangled photons, are reproduced with a classical pseudothermal light source [7, 8, 9]. However, the nature of the spatial correlations exhibited with a pseudothermal source, and whether they can be interpreted as classical intensity correlations [1, 11, 13] or are fundamentally non-local quantum correlations [10, 15], is still under debate.

In this Letter we experimentally study *computational ghost imaging*, a novel ghost imaging technique recently proposed by Shapiro [16]. In this technique the multipixel detector is replaced with a 'virtual detector', by calculating the propagation of the field of the reference beam. The image is reconstructed by correlating the calculated field patterns with the measured intensities at the object arm. Our measurements show that pseudothermal-light GI and GD can be performed with only one beam and one detector. As noted by Shapiro, this proves that GI cannot possibly depend on any non-local quantum correlations. We also demonstrate scanningless 3D sectioning

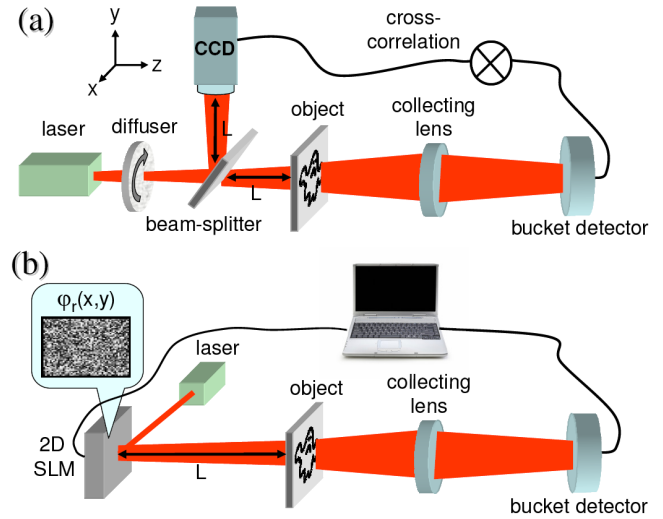


Figure 1: (Color online) Experimental setups for ghost imaging: (a) The standard pseudothermal two-detectors setup, where a ghost-image of the object is obtained by correlating the pseudothermal field measured by a CCD with the intensity measured by a bucket detector. (b) The computational single-detector setup used in this work. A pseudothermal light beam is generated by applying controllable phase masks $\varphi_r(x,y)$ with a spatial light modulator (SLM). The object image is obtained by correlating the *calculated* field with the intensity measured by the bucket detector.

capability of this technique.

Computational GI can be considered as a variant of the standard two-detectors pseudothermal GI. In pseudothermal GI, a spatially incoherent beam is generated by passing a laser beam through a rotating diffuser (Fig. 1a). The beam is then split on a beam-splitter, generating the two spatially correlated beams required for GI. The essence of computational GI is to replace the rotating diffuser with a computer controlled spatial light modulator (SLM), which serves as a controlled phase-mask for the spatial phase of the light field $\varphi(x,y)$ (Fig 1b). A spatially incoherent beam is generated by applying pseudo-random phase patterns $\varphi_r(x,y)$ on the SLM. Since for each phase realization r the controlled phase pattern is known, one can evaluate the field right after the SLM, $E_r(x,y,z=0) = E^{(in)} e^{i\varphi_r(x,y)}$ (where $E^{(in)}$ is the incident field on the SLM). Knowing $E_r(x,y,z=0)$,

^{*}yaron.silberberg@weizmann.ac.il

the field at any distance z from the SLM can be computed using the Fresnel-Huygens propagator:

$$E_r(x, y, z) = \int d\xi d\eta E_r(x - \xi, y - \eta, 0) e^{i\frac{2\pi}{\lambda z}(\xi^2 + \eta^2)}, \quad (1)$$

where λ is the wavelength of the source. In order to reconstruct the transmission function of an object $T(x, y)$ placed at $z = L$, the *computed* intensity patterns at the object plane $I_r = |E_r(x, y, z = L)|^2$ are cross-correlated with the intensities *measured* by the bucket detector placed behind the object $B_r = \int dx dy I_r(x, y, L) T(x, y)$:

$$\begin{aligned} G(x, y) &\equiv \frac{1}{N} \sum_{r=1}^N (B_r - \langle B \rangle) I_r(x, y) \\ &= \langle B I(x, y) \rangle - \langle B \rangle \langle I(x, y) \rangle. \end{aligned} \quad (2)$$

Where $\langle \cdot \rangle \equiv \frac{1}{N} \sum_r \cdot$ denotes an ensemble average over N phase realizations. Intuitively, one can see that the image is obtained by summing the calculated intensities I_r with the appropriate weights B_r : The larger the overlap between the generated intensity pattern and the transmission object, the higher is the intensity measured by the bucket detector B_r , and thus the calculated $I_r(x, y)$ is summed with a larger weight. It is important to note that in conventional GI the object is also reconstructed according to Eq. (2). The only difference is that here $I_r(x, y, z = L)$ are *computed*, whereas in conventional GI I_r are obtained by measuring the intensities at the reference arm using a multipixel detector placed at a specific distance $z = L$. Thus, similar to what is well known for conventional GI, one can show that $G(x, y)$ is given by the transmission function of the object convolved with the coherence function of the field at the plane of the object [1, 13]. The resolution of the reconstructed object is therefore limited by the coherence area of the field at the object plane.

To demonstrate computational GI experimentally, we have constructed the setup presented in Fig. 1b. The setup is based on a two-dimensional phase-only liquid crystal on silicon spatial-light-modulator (LCOS-SLM, Holoeye HEO1080P), with 1080x1920 addressable $8\mu\text{m} \times 8\mu\text{m}$ pixels. The computer controlled 2D-SLM is illuminated by a CW Helium-Neon laser, which produces a Gaussian beam with a waist of $w_0 = 740\mu\text{m}$ on the 2D-SLM plane. A $2\text{cm} \times 2\text{cm}$ object (transmission plate) is placed at distance $L = 84\text{cm}$ from the SLM, and a lens collects the transmitted light onto the bucket detector. In each realization a mask of 300×300 random phases is sent to the SLM, where each phase is realized by 3×3 SLM pixels. The reconstructed image using 16000 realizations is shown in Fig. 2a, displaying the accurate reconstruction of the object transmission $T(x, y)$ (Fig. 2a, inset). This experimental result cannot be attributed to nonlocal quantum correlations, since only a single detector was used. We note that one can reconstruct an object placed at any distance L from the source, both in the near- and

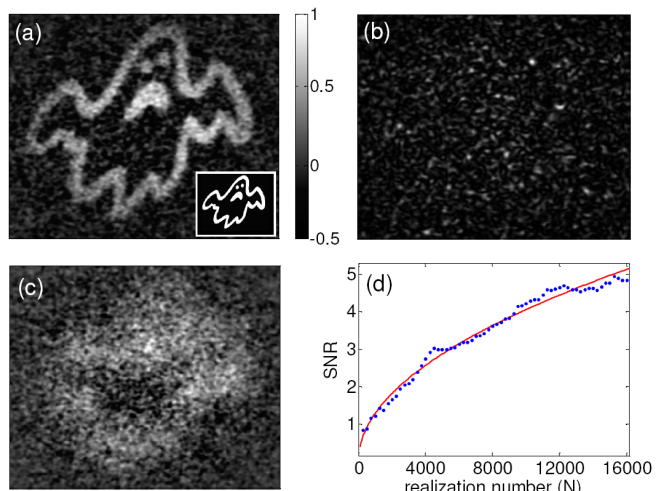


Figure 2: (Color online) Computational ghost-image reconstruction of a $2\text{cm} \times 2\text{cm}$ transmission mask placed at $L = 84\text{cm}$. (a) Reconstructed image at the object plane, obtained with 16000 realizations. The inset shows the transmission mask. (b) A calculated intensity pattern of a single phase realization. The resolution of the reconstruction in (a) is dictated by the speckle size. (c) Reconstructed out-of-focus image, at a different z -plane ($L = 24\text{cm}$), demonstrating the depth-resolving capabilities of the computational method. (d) Measured SNR of the reconstructed image as a function of the number of realizations (blue dots). The theoretical line depicts \sqrt{N} dependence.

far-field zones, as long as the field at the object plane can be calculated using Eq. (1). This is demonstrated below, with an object placed at $L = 11\text{cm}$.

An intensity pattern calculated from a *single* realization is shown in Fig. 2b, revealing the speckle field that impinges on the object for this specific realization of random phases [17]. Reconstruction of an image at a z -plane different than the actual location of the object, results in an out-of-focus image of the object, indicating the depth-resolving capabilities of computational GI (Fig. 2c). This is analogous to scanning the z -position of the multipixel detector in conventional GI, but is performed here for all z -locations simultaneously, without the need for additional measurements. This feature allows for a full three-dimensional reconstruction of the object field, with the only price of executing more calculations.

Since the computational GI scheme is completely analogous to pseudothermal GI, the two techniques share similar resolution and signal-to-noise (SNR) properties [16, 17, 18, 19]. To summarize these, the transverse resolution is determined by the coherence length (speckle size) at the object plane, which is given by the Van-Cittert Zernike theorem $\delta x(z) = \lambda z / \pi w_0$. The depth resolution is given by $\delta z(z) = 2\pi \delta x^2 / \lambda$. For the presented experimental parameters, $\delta x(L = 84\text{cm}) = 230\mu\text{m}$ and $\delta z(L = 84\text{cm}) = 50\text{cm}$, in agreement with the experimental results. In pseudothermal GI, the SNR scales as the square-root of the ratio of the number of realiza-

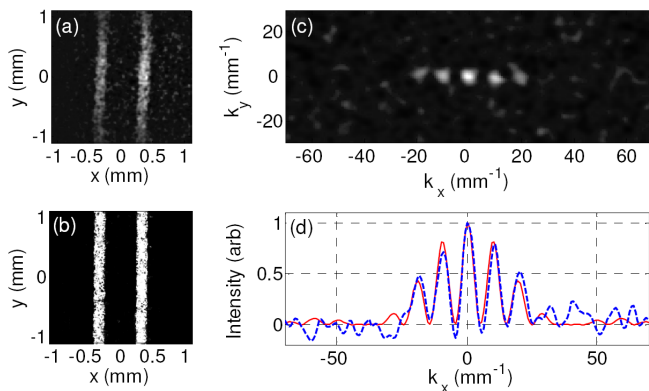


Figure 3: (Color online) Simultaneous reconstruction of an object and its diffraction pattern, with 8000 realizations. (a) Reconstructed ghost image of a two-slit transmission plate. The resolution of the image is determined by the speckle size, $\delta x \sim 0.018\text{mm}$ (b) Transmission microscope image of the double-slit slide. The width of each slit is $170\mu\text{m}$ and the separation is $400\mu\text{m}$. (c) Ghost diffraction pattern reconstructed using a pinhole detector. The resolution of the diffraction image is $\delta k \sim 1.4\text{mm}^{-1}$, lower than the Fourier limit $\delta x \delta k < 0.5$. (d) A cross-section of the ghost diffraction pattern shown in (c) (dashed blue), and the theoretical two-slit diffraction pattern calculated from the dimensions of the double-slit (red).

tions N and the average number of speckles transmitted through the object N_s , $\text{SNR} \propto \sqrt{N/N_s}$ [18, 19]. Since N_s is given by the ratio of the object transmissive area to the coherence area, there is a clear trade-off between resolution and SNR. The SNR as a function of the number of realizations for the reconstructed image of Fig. 2a, is presented in Fig. 2d, in agreement with the theoretical prediction. A movie visualizing the image build-up can be found at [20].

One of the features in common to ghost imaging with a nonclassical source and a pseudothermal source, is the ability to resolve both the object and its diffraction pattern with high resolution. In conventional GD, the diffraction pattern of the object is reconstructed by replacing the bucket detector with a small single-pixel ('pinhole') detector, placed at the Fourier plane of the collecting lens [6, 8]. The GD is reconstructed by correlating the intensities measured by the pinhole detector with the diffraction pattern of the field in the reference arm. In fact, both the near-field object image (GI) and its diffraction pattern (GD) can be obtained by changing only the optical setup at the reference arm. In our single detector configuration, since the reference arm is virtual, the only required change is in the computational procedure. One can therefore perform GI and GD si-

multaneously, with a single set of measured data (i.e. the intensities measured with the pinhole detector B_r). Both images are reconstructed using Eq. (2), where for GI I_r is computed according to Eq. (1), and for GD I_r is obtained by calculating the Fourier transform (FT) of $E_r(x, y, z = 0)$, $I_r = |\text{FT}(E_r(x, y, z = 0))|^2$. The intensities measured by a pinhole detector placed on the optical axis are given by $B_r = |\int dx dy E_r(x, y, L) T(x, y)|^2$. We note that by using a pinhole detector instead of a bucket detector, the SNR of the GI is degraded, since only a small fraction of the transmitted light is collected.

In order to demonstrate the simultaneous reconstruction of GI and GD, we have placed a double-slit transparency at $L = 11\text{cm}$ from the SLM and a small pinhole detector at the Fourier plane of the collecting lens (a single $8.6\mu\text{m} \times 8.4\mu\text{m}$ pixel of a CCD camera). We reconstructed the double-slit diffraction pattern using the pinhole-detector measured intensities, and its transmission image using a bucket-detector measured intensities (summing over the CCD's pixels), obtained simultaneously with the same phase realizations. We have also used the pinhole detector to reconstruct both the GD and GI, but with much lower SNR for the latter (not shown). Fig. 3 summarizes the results of the near-field and far-field image reconstructions for the double slit transparency, obtained with 8000 realizations. Comparing Fig. 3a and Fig. 3d, it is obvious that the product of the resolution of the near-field image (δx) and of the far-field image ($\delta k \sim 1/w_0$) is much smaller than the Fourier limit, i.e. $\delta x \delta k = 0.025 \ll 0.5$. This cannot be obtained by simply scanning the object with a coherent laser beam [6]. However, it does not violate the Einstein-Podolsky-Rosen (EPR) bound for classical light, as was previously shown with a pseudothermal source [8]. Knowing both the near- and far-field intensity patterns with high-resolution enables the reconstruction of the object's transmission amplitudes *and* phases, using the Gerchberg Saxton phase-retrieval algorithm [21]. This ability of computational GI might be appealing for phase sensitive applications.

Finally, we note that in computational GI the main complexity is shifted from the experimental apparatus, to the calculation. Thus, it allows for 3D reconstruction by only post processing the retrieved data, eliminating mechanical scans. One might consider applying computational GI for other 3D imaging tasks which are not necessarily transmission-based. Two examples for such are radar applications, and scanningless depth-resolved microscopy using fluorescent probes. Furthermore, the use of a SLM enables the implementation of closed-loop feedback schemes, potentially reducing the number of realizations needed for image reconstruction.

[†] equally contributed

[1] A.Gatti, M. Bache, D. Magatti, et al., J. Mod. Opt., **53**,

739 (2006); A. Gatti, E. Brambilla, and L. A. Lugiato, in Progress in Optics, edited by E. Wolf (Elsevier, Ams-

- terdam, 2008), Vol. **51**, p. 251.
- [2] T. B. Pittman, Y. H. Shih, D. V. Strekalov, et *al.*, Phys. Rev. A **52**, R3429 (1995).
- [3] D. V. Strekalov, A. V. Sergienko, D. N. Klyshko, and Y. H. Shih, Phys. Rev. Lett. **74**, 3600 (1995).
- [4] R.S. Bennink, S. J. Bentley and R.W. Boyd, Phys. Rev. Lett. **89**, 113601 (2002).
- [5] A. Gatti, E. Brambilla and L. A. Lugiato, Phys. Rev. Lett. **90**, 133603 (2003).
- [6] R. S. Bennink, S. J., Bently, R. W. Boyd, et *al.*, Phys. Rev. Lett. **92**, 033601 (2004).
- [7] A. Gatti, E. Brambilla, M. Bache, et *al.*, Phys. Rev. Lett. **93**, 093602 (2004).
- [8] F. Ferri, D. Magatti, A. Gatti, et *al.* Phys. Rev. Lett. **94**, 183602 (2005).
- [9] A. Valencia, G. Scarcelli, M. D'Angelo, and Y. Shih, Phys. Rev. Lett. **94**, 063601 (2005).
- [10] G. Scarcelli, V. Berardi, and Y. Shih, Phys. Rev. Lett. **96**, 063602 (2006); G. Scarcelli, V. Berardi, and Y. H. Shih Phys. Rev. Lett. **98**, 039302 (2007).
- [11] A. Gatti, M. Bondani, L. A. Lugiato, M. G. A. Paris, and C. Fabre, Phys. Rev. Lett. **98**, 039301 (2007); A. Pe'er, arXiv 0605131 (2006).
- [12] L. Basano and P. Ottonello, Opt. Exp. **15**, 12386-12394 (2007).
- [13] B. I. Erkmen and J. H. Shapiro, Phys. Rev. A. **77**, 043809 (2008).
- [14] R. Meyers, K. S. Deacon, and Y. Shih, Phys. Rev. A **77**, 041801(R) (2008).
- [15] Y. Shih, IEEE J. Sel. Top. Quantum Electron. **13**, 1016 (2007); Y. Shih, arXiv:0805.1166v1 (2008)
- [16] J. H. Shapiro, to be published in Phys. Rev. A, arXiv:0807.2614 (2008).
- [17] J. W. Goodman, Speckle Phenomena in Optics. Roberts & Co., Greenwood Village, CO, 2007
- [18] A. Gatti, D. Magatti, and F. Ferri, Phys. Rev. A **78**, 063806 (2008).
- [19] B. I. Erkmen, J. H. Shapiro, arXiv:0809.4167v1 (2008).
- [20] See <http://www.weizmann.ac.il/home/feori/Misc.html> for a movie visualizing the image build-up.
- [21] R. W. Gerchberg and W. O. Saxton, Optik (Stuttgart) **35**, 237-246 (1972).